Infrared Action Spectroscopy and Dissociation Dynamics of the HOOO Radical

Erika L. Derro, Craig Murray, Timothy D. Sechler, and Marsha I. Lester*

Department of Chemistry, University of Pennsylvania, Philadelphia, Pennsylvania 19104-6323

Received: July 31, 2007; In Final Form: September 14, 2007

The HOOO radical has long been postulated to be an important intermediate in atmospherically relevant reactions and was recently deemed a significant sink for OH radicals in the tropopause region. In the present experiments, HOOO radicals are generated in a pulsed supersonic expansion by the association of O_2 and photolytically generated OH radicals, and the spectral signature and vibrational predissociation dynamics are investigated via IR action spectroscopy, an IR-UV double resonance technique. Rotationally resolved IR action spectra are obtained for *trans*-HOOO in the fundamental (ν_{OH}) and overtone ($2\nu_{OH}$) OH stretching regions at 3569.30 and 6974.18 cm^{-1}, respectively. The IR spectra exhibit homogeneous line broadening, characteristic of a ~26-ps lifetime, which is attributed to intramolecular vibrational redistribution and/or predissociation to OH and O_2 products. In addition, an unstructured feature is observed in both the OH fundamental and overtone regions of HOOO, which is likely due to *cis*-HOOO. The nascent OH $X^2\Pi$, $v = 0$ or $v = 1$, products following vibrational predissociation of HOOO, ν_{OH} or $2\nu_{OH}$, respectively, have been investigated using saturated laser-induced fluorescence measurements. A distinct preference for population of $\Pi(A')$ Λ-doublets in OH was observed and is indicative of a planar dissociation of *trans*-HOOO in which the symmetry of the bonding orbital is maintained.

Introduction

The potential importance of the HOOO radical as an intermediate in disparate areas such as fundamental gas-phase reactions, antibody-catalyzed oxidation of water as a means of killing bacteria,[1] and the ozonation of various organic molecules[2−4] has brought much attention recently. The existence of the HOOO radical has significant bearing on atmospheric chemistry, as it has been implicated as an intermediate in several key atmospheric reactions and relaxation processes. Highly vibrationally excited OH is produced in the reaction of ozone with atomic hydrogen[5,6]

$$H + O_3 \rightarrow OH\ (v \leq 9) + O_2 \qquad \text{(R1)}$$

Subsequent fundamental and overtone vibration−rotation transitions ($\Delta v \geq 1$) give rise to visible and near-IR emission, and this chemiluminescence is responsible for the Meinel bands that dominate mesospheric airglow.[7] The high degree of vibrational excitation is indicative of a strongly attractive potential energy surface, consistent with the presence of an attractive well in the exit channel. Collisional deactivation of vibrationally excited OH by O_2

$$OH\ (v) + O_2 \rightarrow OH\ (v - 1) + O_2 \qquad \text{(R2)}$$

has been investigated by a number of researchers[8−11] and is the major removal process for vibrationally excited OH produced by R1 in the atmosphere. Recently, McCabe et al.[11] measured rate coefficients for vibrational relaxation of OH $X^2\Pi$ $v = 1$ over a range of temperatures. The negative temperature dependence observed indicates that attractive forces dominate and strongly suggests that relaxation proceeds via formation of the HOOO intermediate. It was argued that the relaxation kinetics are governed by a competition between intramolecular vibrational redistribution (IVR) of HOOO and dissociation of the intermediate.[11]

A key reaction in the atmospheric HO_x cycle

$$O + HO_2 \rightarrow OH + O_2 \qquad \text{(R3)}$$

can in principle proceed either via hydrogen abstraction or by way of a HOOO intermediate. An elegant laser-induced fluorescence study[12] using isotopically labeled ^{18}O showed conclusively that R3 occurred via a HOOO intermediate quantitatively. Furthermore, and perhaps most importantly, we have recently shown that HOOO is relatively stable with respect to the OH + O_2 asymptote.[13] Thus, it may act as a temporary sink for OH radicals and be present in measurable concentrations in the earth's atmosphere.

Experimentally, HOOO proved elusive until fairly recently, and the literature is limited. Cacace et al. provided the first conclusive evidence for HOOO being stable with direct detection in a multisector mass spectrometer.[14] Protonated ozone, HO_3^+, was produced via chemical ionization and subsequently collisionally neutralized and then reionized before being detected as a recovery signal at the $m/z = 49$ parent ion position in the mass spectrum. The delay between the neutralization and reionization steps was of the order of microseconds, indicating that HOOO was stable on this time scale. Direct spectroscopic observation of HOOO was initially accomplished in an Ar matrix by Nelander and co-workers shortly afterward.[15] Transitions at 3361, 1223, and 556 cm^{-1} were assigned, in conjunction with the analogous transitions in isotopically substituted HOOO, to the fundamental OH stretch, HOO bend, and OOO bend modes, respectively. The fundamental HOO bend transition has also been observed at 1259 cm^{-1} in irradiated H_2O−ice by Cooper et al.[16] and very recently by Zheng et al.[17]

* Corresponding author. Telephone: (215) 898-4640. Fax: (215) 573-2112. E-mail: milester@sas.upenn.edu.

10.1021/jp0760915 CCC: $37.00
Published on Web 10/24/2007

The Fourier-transform microwave (FTMW) study presented by Suma et al.[18] was the first direct, gas-phase spectroscopic observation of HOOO. The radical was produced by electrical discharge of a free-jet expansion of water seeded in O_2/Ar carrier gas. The observed rotational transitions were assigned to the *trans*-HOOO conformer, with the assistance of rotational constants obtained from multireference configuration interaction (MRCI) calculations. The observed inertial defect furthermore confirmed the planarity of *trans*-HOOO, and a fairly long central O−O bond length, r_{O-O}, of 1.688 Å was found. Subsequently, we reported observation of HOOO in a supersonic free-jet using IR action spectroscopy.[13] The OH stretch overtone, $2\nu_{OH}$, was excited using tunable IR radiation, and the nascent OH $X^2\Pi$ products were probed using laser-induced fluorescence excitation spectroscopy. Analysis of the energetically highest open product channel allowed the determination of an upper limit for the dissociation energy; we found $D_0 \leq 2140$ cm^{-1} or 6.12 kcal mol^{-1}. This is an especially important experimental quantity, as it is the major factor contributing to thermodynamic estimations of the relative abundance of HOOO in the atmosphere. A statistical mechanical analysis using this upper limit D_0 indicated that up to 66% of atmospheric OH may exist in the form of HOOO in the vicinity of the tropopause. The only other experimental measurement of the dissociation energy is by Speranza,[19] who examined the electron-transfer efficiency between $HOOO^+$ and a series of neutrals to determine an enthalpy of formation $\Delta_f H_{298K} = -1 \pm 5$ kcal mol^{-1} for HOOO, implying a stability of 10 ± 5 kcal mol^{-1}. The limiting value for D_0 obtained from the IR action spectroscopy experiment[13] provides a refinement to the previous experimental measurement, implying that $\Delta_f H_{298K} \geq 1.68$ kcal mol^{-1}.

Generally, the agreement between experimental and theoretical thermochemistry for HOOO is poor. Using isodesmic reactions, Denis et al. recommended a value of $\Delta_f H_{298K} = 6.3 \pm 2.0$ kcal mol^{-1}, wherein individual enthalpies were computed at the DFT or CCSD(T)/CBS level of theory.[20] This value is in agreement with the older calculations of $\Delta_f H_{298K}$ for HOOO of Jungkamp and Seinfeld (6.1 kcal mol^{-1}),[21] Yu and Varandas (4.17 kcal mol^{-1}),[22] and Setokuchi et al. (5.23 kcal mol^{-1});[23] however, it is in marked disagreement with the value reported by Speranza,[19] and it underestimates the stability recently derived by Murray et al.[13] Fabian et al. argued that the similarity of the underlying method may be responsible for the apparent convergence between the calculated enthalpies of formation.[24]

One possible explanation for the lack of agreement between experiment and theory is the comparatively low-level molecular geometries used in most theoretical model chemistries. Optimized geometries of HOOO are strongly dependent on both method and basis set, and most commonly used methods fail to predict a structure consistent with that reported in the FTMW study. Specifically, the central O−O distance is most sensitive to the method of calculation and can be underestimated by up to 0.3 Å when single reference methods are used. For example, when using a moderate cc-pVTZ basis set, the calculated central O−O bond length for *trans*-HOOO varies from 1.437 Å at the MP2 level, 1.475 Å at the QCISD level, 1.544 Å at the B3LYP level to 1.75 Å at the CASSCF level.[23] In general, multireference methods predict longer central O−O bond lengths in HOOO, and this is consistent with the results of ab initio calculations on its halogenated analogue FOO,[25] for which there exist similar discrepancies between the experimental and theoretical thermochemistry. The extreme variability between different levels of theory (in geometry, stability, and relative stability of the cis and trans conformers) and discrepancies throughout these computational studies in the literature highlights the need for experimental measurements to adequately characterize HOOO and provide checks on theory.

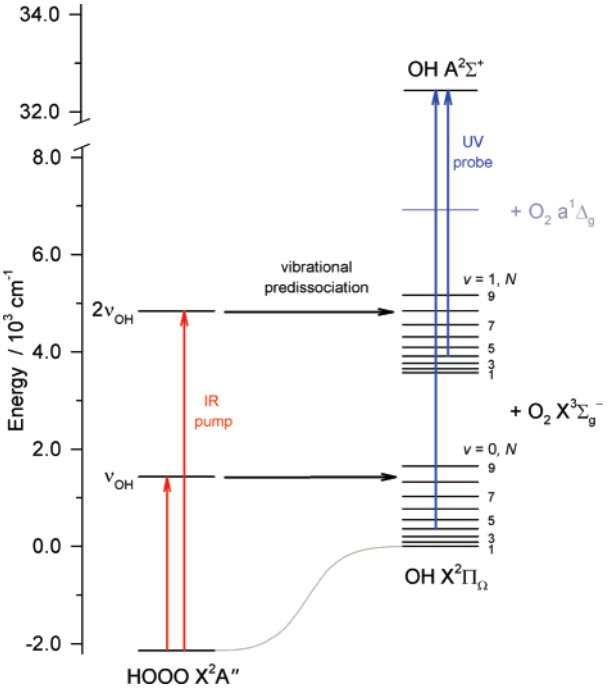

Figure 1. Schematic illustrating the energetics of HOOO relative to the OH $X^2\Pi$ + O_2 $X^3\Sigma_g^-$ asymptote and the experimental IR pump−UV probe approach. HOOO is vibrationally excited to ν_{OH} or $2\nu_{OH}$ with an IR laser, causing vibrational predissociation, which occurs exclusively with loss of a single quantum of OH stretch excitation. The nascent OH products are subsequently detected with a UV probe by laser-induced fluorescence on the A−X transition.

In this article, we report a detailed analysis of the IR action spectrum of the HOOO radical in the fundamental and overtone OH stretch regions and fine-structure resolved measurements of nascent OH $X^2\Pi$ vibrational predissociation products. These results are discussed with respect to the nature of the chemical bonding in HOOO $\tilde{X}^2A''$.

Experimental Section

HOOO radicals are readily formed following three-body association of OH and O_2 radicals in the collisional region of a pulsed free-jet expansion. OH is produced by photolysis of $HONO_2$, which is seeded in a mixture of O_2 (20% by volume) and Ar (balance) at a backing pressure of 50 psi, using the 193-nm output of an ArF excimer laser (Lambda Physik Compex 102). Photolysis occurs directly beyond the aperture of the pulsed valve (General Valve Series 9, $D = 0.8$ mm) in the throat of the expansion, and collisions with the carrier gas stabilize newly formed HOOO. The excimer laser beam diameter is restricted to 3 mm using an iris rather than by focusing, which limits the laser fluence to ~10 mJ cm^{-2}. This was found to have the twin benefits of reducing the residual OH background while simultaneously enhancing the production of HOOO relative to harsher photolysis conditions.

IR action spectra of HOOO and the OH $X^2\Pi$ product state distributions following vibrational predissociation were recorded using an IR pump−UV probe technique, as illustrated schematically in Figure 1. Counterpropagating and spatially overlapped pulsed IR and UV laser beams, both of which are gently focused to beam diameters of approximately 2 mm, interrogate the free-jet expansion 15 nozzle diameters ($x/D = 15$) downstream. The

IR beam excites the OH stretch fundamental (ν_{OH}) or overtone ($2\nu_{OH}$) of HOOO at ~2.8 or ~1.4 μm, respectively, and the UV beam state selectively probes the OH $X^2\Pi$ products of vibrational predissociation after a delay of 50 ns. Tunable IR radiation of 0.15 cm^{-1} bandwidth is generated in an optical parametric oscillator (OPO, LaserVision), pumped by an injection seeded Nd:YAG laser (Continuum Precision II 8000, 10 Hz). Frequency calibration is accomplished while recording spectra by monitoring the frequency of the unused signal wave from the oscillator stage of the OPO, using a wavemeter (Coherent Wavemaster), in conjunction with prior knowledge of the absolute frequency of the pump beam. It was necessary to purge the IR beam path with N_2 while recording the ν_{OH} IR spectrum of HOOO to avoid water absorption in the 2.8-μm region. The frequency-doubled output of a Nd:YAG pumped dye laser (Continuum Surelite II and ND6000, 20 Hz) provides the UV laser beam for OH detection by laser-induced fluorescence (LIF).

The probe laser state selectively excites OH on selected $A^2\Sigma^+ - X^2\Pi$ (1,0) or (1,1) transitions at ~283 and ~315 nm, and the resulting fluorescence is collimated using a f/1 lens and refocused at a 1-mm wide slit using a f/2 lens, ensuring that only the colder central region of the free-jet is imaged. Wavelength discrimination and suppression of scattered probe laser light is achieved using narrow band interference filters, which in some cases were used in combination with a high reflector for added wavelength selectivity before impinging upon a photomultiplier tube (Electron Tubes 9813QB). The signal from the photomultiplier was preamplified and displayed on a digital storage oscilloscope (LeCroy WaveRunner 6050A) interfaced with a PC for further processing.

Results and Discussion

A. IR Action Spectra: *trans*-HOOO. IR action spectra were recorded by scanning the IR laser frequency while the probe laser remained fixed at a known OH $A^2\Sigma^+ - X^2\Pi$ transition. The choice of OH transition for acquisition of action spectra is dictated by the product state distribution and a compromise between absolute magnitude of the IR-induced LIF signal and that due to residual OH background. As the pump−probe detection of HOOO takes place in the effectively collision-free region of the supersonic expansion, the residual hydroxyl radicals are jet-cooled and found almost exclusively in the lowest rotational level of the ground spin−orbit state OH $X^2\Pi_{3/2}$, $N = 1$ in both $v = 0$ and $v = 1$, although a high N tail persists. The residual population in $v = 0$ is vastly greater than that in $v = 1$. Excitation of $2\nu_{OH}$ was found to result exclusively in OH $X^2\Pi$, $v = 1$ products, while ν_{OH} excitation necessarily can result in only OH $X^2\Pi$, $v = 0$ predissociation products, as indicated schematically in Figure 1. The product state distributions will be discussed in detail in the subsequent section, but the peak signal intensities were observed using the $P_1(4)$ transitions of the $A^2\Sigma^+ - X^2\Pi$ (1,0) and (1,1) bands, and these transitions were used to record the action spectra.

Partially rotationally resolved IR action spectra were observed for HOOO under jet-cooled conditions at 3569.30 ± 0.05 and at 6974.18 ± 0.05 cm^{-1}, which are band origins as determined from fits to the spectra (vide infra). These transitions are assigned to the fundamental OH stretch and overtone OH stretch in HOOO, respectively, based on their vibrational frequencies, which are only shifted slightly from the free OH radical (ν_{OH} = 3568.47 cm^{-1} and $2\nu_{OH}$ = 6971.35 cm^{-1}).[26] The spectra are displayed in their entirety in Figure 2 as a function of relative wavenumber with the respective band origins set to 0 cm^{-1}.

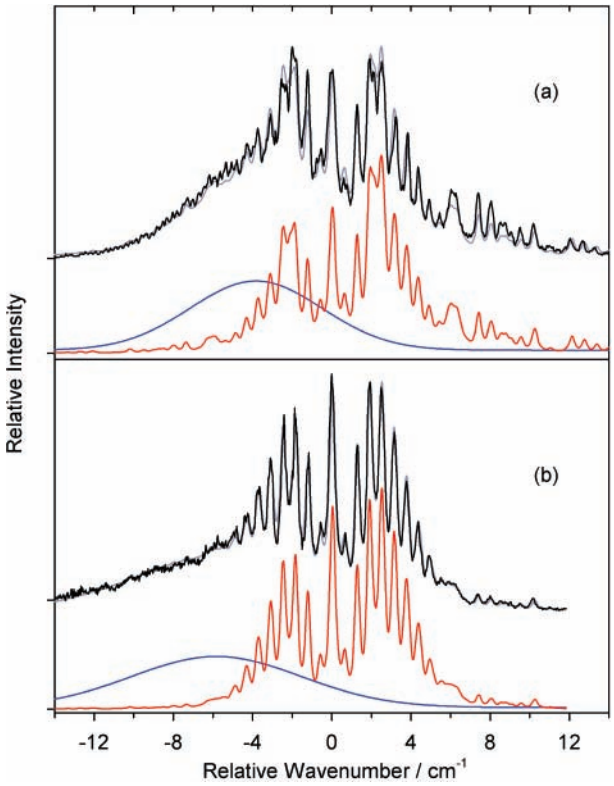

Figure 2. Experimental IR action spectra (black) and simulations of the HOOO radical in (a) the ν_{OH} and (b) the $2\nu_{OH}$ regions recorded with the probe laser fixed on the $P_1(4)$ transition of the OH $A^2\Sigma^+ - X^2\Pi$ (1,0) and (1,1) bands, respectively. The wavenumber scale has been adjusted such that the band origins of the structured features, assigned to ν_{OH} and $2\nu_{OH}$ of *trans*-HOOO conformer at 3569.30 ± 0.05 and 6974.18 ± 0.05 cm^{-1}, respectively, are set to 0 cm^{-1}. The total simulations (gray) are the respective sums of the structured *trans*-HOOO simulations (red) and a line shape function (blue) used to represent the unstructured feature, which is assigned to the *cis*-HOOO conformer.

The spectra in both the ν_{OH} and $2\nu_{OH}$ regions comprise a rotationally structured band and an unstructured component shifted to lower wavenumber. The structured portion will be the focus of this section, while the unstructured component will be considered in subsection C.

Figure 3 shows an expanded view of the rotationally structured portion of the IR action spectrum obtained in the $2\nu_{OH}$ region. The rotational structure was simulated for the $^2A''$ radical using Pickett's SPCAT program for asymmetric rotors.[27] The experimental spectrum has been modified by subtracting out the contribution from the unstructured component to enable straightforward comparison to the simulations. The top panel contains a simulation using calculated rotational constants for *cis*-HOOO from the geometry optimized in the MRCI calculations of Suma et al.,[18] and the lower panel contains a simulation using analogous calculated *trans*-HOOO rotational constants. These simulations were generated using the same rotational constants for both lower and upper states, initially assuming they do not change upon OH vibrational excitation. In both cases, the band origin is fixed at the experimental value. The line positions in the *cis*-HOOO simulation are in poor agreement with the experiment, whereas the trans simulation reproduces the experimental line positions very well. Rotational constants resulting from other calculations with shorter central O−O bond lengths produce simulations that do not agree with our experiment. The positions of the observed rotational features are most

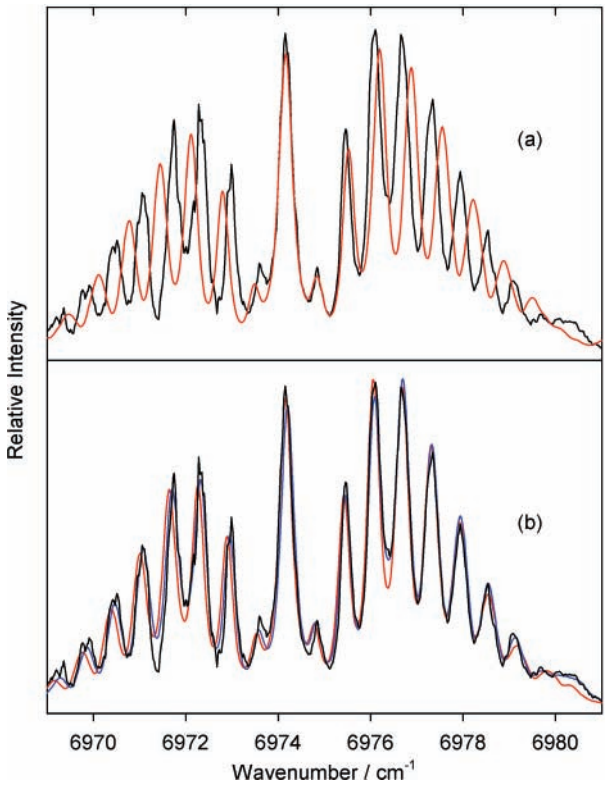

Figure 3. Structured portion of the OH stretch overtone spectrum of HOOO with *cis* (top) and *trans* (bottom) rotational constants used for simulations. The experimental spectrum (black) has been modified by subtracting out the unstructured feature to enable straightforward comparison to the simulations. Simulations (red) are generated using calculated rotational constants for *cis*- and *trans*-HOOO, while the blue line represents a simulation using the experimental rotational constants for *trans*-HOOO from Suma et al.[18] with central O−O bond length of 1.688 Å. Based on the excellent agreement between line positions in the experiment and *trans*-HOOO simulation, the structured portion of the spectrum is assigned to the *trans* conformer.

strongly dependent on the magnitudes of the *B* and *C* rotational constants, which are in turn sensitive to the length of the central O−O bond.

Moreover, the spectral signature observed in our experiment is consistent with rotational constants derived previously in the FTMW experimental study of Suma et al.,[18] and the agreement is displayed in the lower panel of Figure 3. Briefly, the rotational transitions observed in the FTMW were definitively assigned to *trans*-HOOO for two reasons. First, a- and b-type rotational transitions were observed with comparable intensities, which is consistent with the calculated magnitudes of the a- and b-components of the permanent dipole moment of the trans conformer. For *cis*-HOOO, significantly more intense b-type transitions would have been expected, since the projection of the dipole moment onto the *b*-axis is much greater than the projection onto the *a*-axis. Second, the experimentally observed rotational constants for HOOO and DOOO are in better agreement with the calculated MRCI constants for the trans conformer for both isotopes. The remarkable agreement between the present experiments and the results of the FTMW experiment identifies the structured bands in both the ν_{OH} and $2\nu_{OH}$ regions as *trans*-HOOO.

Accordingly, the structured bands in the experimental spectra are simulated using the experimentally determined rotational constants for *trans*-HOOO $\tilde{X}^2A''$.[18] Inclusion of additional molecular parameters, such as centrifugal distortion, spin rotation, and magnetic dipole−dipole coupling constants, did not have a noticeable effect on the simulation at our resolution, which is limited by homogeneous line broadening, given that only the lowest *N* levels are populated at the low temperature (∼9 K) in the supersonic jet. Therefore, only rotational constants were included in the simulations. Furthermore, there is no observable change in rotational constants for *trans*-HOOO ($2\nu_{OH}$) as compared with ν_{OH} and the ground state of *trans*-HOOO, indicating minimal structural changes upon vibrational excitation of the OH stretching mode. Using the spectroscopic constants indicated above for *trans*-HOOO, we varied the vibrational band origin, Lorentzian line width, rotational temperature, and the transition dipole moment ratio (denoted as an a/b ratio for a planar molecule) in a least-squares fitting procedure to match the intensities and line widths in the experimental spectra.

The line width in the action spectra contains information about the decay dynamics of HOOO following vibrational excitation. In both spectra, there is significant homogeneous line broadening beyond the OPO laser bandwidth of 0.15 cm^{-1}. A careful power dependence study was performed to ensure that the spectra were recorded in a linear regime and not power broadened. Reduction of IR laser power did not result in a measurable decrease in the homogeneous line width of the spectra. The fits to the spectra yielded Lorentzian line widths of 0.212 ± 0.008 cm^{-1} for the OH fundamental and 0.207 ± 0.006 cm^{-1} for the overtone. The uncertainties represent 2σ standard deviations. The line widths correspond to lifetimes of 25 ± 1 and 26 ± 1 ps for *trans*-HOOO ν_{OH} and $2\nu_{OH}$ states, respectively, and can be attributed to IVR and/or predissociation to OH and O_2 products. Additionally, the appearance of OH products following vibrational predissociation of HOOO was monitored as a function of time delay between the IR pump and UV probe lasers. No enhancement in the OH LIF signal was observed when the UV preceded the IR; however, when the IR and UV lasers were overlapped in time, the OH LIF signal rapidly increased until it leveled off at maximum intensity, indicating that the time domain measurements are limited by the temporal resolution of the laser pulses. Nevertheless, these measurements corroborate dissociation lifetimes of HOOO (ν_{OH}) and ($2\nu_{OH}$) $\leq$ 8 ns, as indicated by the lifetime broadening observed in the IR action spectra.

It is evident when comparing the spectra in Figure 2 that the rotational band contours differ in the OH fundamental and OH overtone transitions, suggesting that the orientation of the transition dipole moment is significantly different for these transitions. Qualitatively, the P-, Q-, and R-branch structure in the $2\nu_{OH}$ spectrum is characteristic of predominantly a-type transitions; however, the more significant presence of b-type transitions in the ν_{OH} spectrum contributes to the intensity observed in the wings, particularly in the high wavenumber portion of the spectrum. To precisely determine the direction of the transition dipole moment relative to the principal inertial axes of *trans*-HOOO, experimental intensities of parallel (a-type) and perpendicular (b-type) transitions are analyzed. The a/b ratio is (1.4 ± 0.1):1 in the OH fundamental spectrum, indicating that the transition dipole moment lies 26° off the OH bond axis, whereas the a/b ratio of (4.9 ± 0.6):1 in the OH overtone spectrum shows that the transition moment lies 52° off the OH bond axis. In both transitions, the ratio of a- to b-type components of the dipole moment is significantly different from that predicted within the bond dipole approximation (a/b = 1:2) for *trans*-HOOO, which assumes that the transition dipole lies along the OH bond axis. The observation of the rotation of the transition moment away from the OH bond axis can be explained by an apparent redistribution of charge with nuclear displace-

ment upon vibrational excitation. Furthermore, the degree of rotation from the OH bond axis increases with increasing vibrational excitation, most likely as a consequence of electrical anharmonicity effects.[28,29]

In each spectral region, the total simulation displayed in Figure 2 is the sum of the rotationally structured *trans*-HOOO simulation and an unstructured component approximated by a simple line shape function, and it is shown as an overlay on the experimental spectrum. There is excellent agreement between the simulations and experimental spectra. The position of the unstructured feature shifts relative to the structured band when going from ν_{OH} to $2\nu_{OH}$. In the OH fundamental spectrum, the unstructured feature is centered 3.9 cm^{-1} to lower wavenumber, while it is shifted 5.9 cm^{-1} to lower wavenumber in the OH overtone spectrum, as displayed in Figure 2. Possible explanations of the origin of this feature will be discussed later.

B. OH $X^2\Pi$ Product State Distributions from *trans*-HOOO Vibrational Predissociation. Nascent OH $X^2\Pi$ vibrational predissociation products were detected following ν_{OH} or $2\nu_{OH}$ excitation of HOOO. This was achieved by fixing the IR laser frequency while scanning the UV probe laser wavelength over fine-structure resolved transitions of the OH $A^2\Sigma^+-X^2\Pi$ band. The IR transition frequencies were selected as the best compromise between absolute signal intensity and optimal discrimination between the structured and unstructured features. Vibrational excitation in the *trans*-HOOO fundamental region was achieved by tuning the IR laser to be resonant with the R(3) transition at 3571.8 cm^{-1}, while the overtone was excited on the analogous transition at 6976.7 cm^{-1}.

OH $X^2\Pi$, $v = 1$ products were detected by exciting on the diagonal $A^2\Sigma^+-X^2\Pi$ (1,1) band and collecting fluorescence on the off-diagonal (1,0) band. For the majority of quantum states in $v = 0$, this detection scheme was simply inverted. Spectral congestion in the excitation step necessitated the use of the (0,0) band for excitation for a small number of quantum states, with subsequent collection of the far weaker off-diagonal (0,1) band. For a given rotational level, *N*, there exist four fine-structure substates which, in the high *J* limit, correspond to $\Pi(A')$ or $\Pi(A'')$ Λ-doublet level levels within both the F_1 and F_2 spin−orbit manifolds. For the most part, fine-structure resolved detection is straightforward, as P- and R-type main branch transitions originate from $\Pi(A')$ levels while Q-type main branch transitions originate from $\Pi(A'')$ levels. Batches of typically four transitions, of which one was a reference for scaling purposes, probing different rotational/fine-structure states were recorded at least three times for the determination of the statistical uncertainty in the signal intensities; the relatively small error bars on the product state distributions, which are shown in Figure 4, are testament to the stability and reproducibility of the fluorescence signals. The intensities were determined from the amplitudes of least-squares fits of the spectral lines. For all transitions probed, the spectral line widths were typically found to be significantly broader than the frequency-doubled dye laser bandwidth, validating the use of saturated LIF population analysis. Conversion of line intensities to ground-state populations followed an analysis procedure described in detail elsewhere[30,31] that incorporates the detection sensitivity, the fluorescence quantum yield, and a degeneracy correction factor.

Vibrational predissociation following excitation of the *trans*-HOOO fundamental band is energetically constrained to produce only OH $X^2\Pi$, $v = 0$ products. By contrast, although $2\nu_{OH}$ excitation can lead to formation of OH $X^2\Pi$ in both $v = 0$ and $v = 1$, we were unable to detect any products in $v = 0$. Thus, vibrational predissociation of the overtone-excited *trans*-HOOO

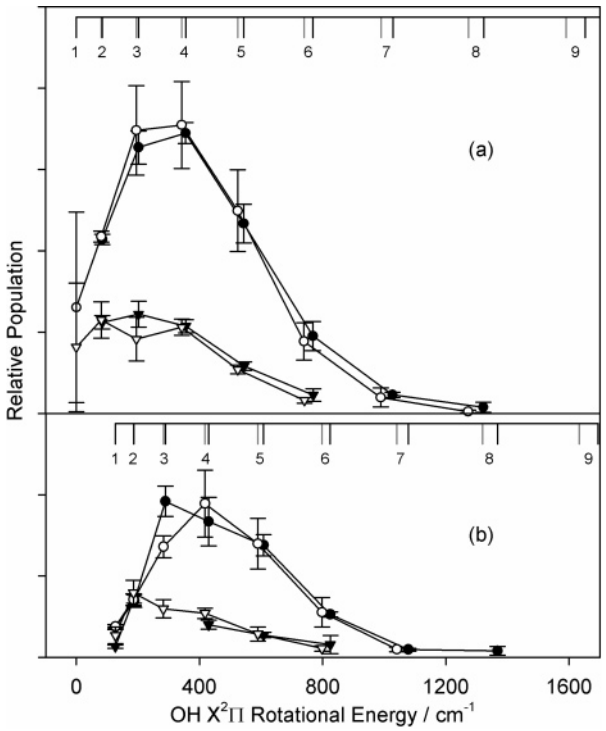

Figure 4. Nascent OH $X^2\Pi$ fine-structure resolved product state distributions as a function of rotational energy in (a) the F_1 and (b) the F_2 spin−orbit manifolds after vibrational excitation of *trans*-HOOO. Excitation of the fundamental OH stretch at 3571.8 cm^{-1} leads to products in $v = 0$, indicated by filled symbols, while overtone excitation at 6976.7 cm^{-1} leads exclusively to $v = 1$ products, indicated by open symbols. Circles represent the populations in F_{1e} and F_{2f} Λ-doublet levels, which can also be identified as $\Pi(A')$, and triangles represent the populations in F_{1f} and F_{2e} levels, also identified as $\Pi(A'')$ (see text). The distributions are normalized to unity over all common fine-structure levels observed, and the error bars represent (2σ) uncertainties from repeated measurements.

occurs exclusively with the loss of one quantum of OH stretch vibration to other degrees of freedom. The broadened spectral line widths of the IR excitations indicate IVR and/or dissociation with similar rapidity upon fundamental and overtone excitation. The remarkable similarity of the OH $X^2\Pi$, $v = 0$ and $v = 1$ rotational distributions from fundamental and overtone excitation displayed in Figure 4 further supports the rapid transfer of one quantum of OH stretch into motion along the dissociative coordinate. The present experiments can be considered as the half-collision analogue of full (i.e., bimolecular) collisions between vibrationally excited OH $X^2\Pi$ with O_2, although the latter process necessarily samples a broader range of initial conditions, including, but not limited to, collision energy, orientation, and impact parameter. Smith and co-workers[11] observed a negative temperature dependence for the relaxation of OH $X^2\Pi$, $v = 1$ by O_2, and thus they argued in favor of formation of a HOOO intermediate in which competition between IVR and redissociation controls the kinetics. Again, the absence of any population in $v = 0$ following excitation of the overtone suggests that IVR is not sufficiently rapid to completely redistribute two quanta of OH stretch vibration before dissociation. Furthermore, the assumption in many kinetic models that vibrational relaxation of OH by O_2 occurs by single quantum $\Delta v = -1$ jumps for low initial v[8−10] is unambiguously validated, at least for $v = 2$, by the present half-collision results. Unfortunately, there are no reported measurements of the rotational or fine-structure distributions of the products of vibrationally inelastic collisions with which to make a comparison.

While a distinct propensity for the production of Π(A′) Λ-doublets is apparent in Figure 4 (vide infra), we start our analysis by modeling the rotational distribution statistically through the use of a prior distribution. For the OH $X^2\Pi$ product levels observed experimentally, the Λ-doublet splitting is small (<5 cm^{-1}) and was therefore initially neglected in the analysis, while the energetic spacing between levels of the same N in each spin−orbit manifold (∼50 cm^{-1} at the highest N) is sufficiently large to be treated explicitly. Consequently, the experimental OH $X^2\Pi$ rotational distributions were summed over Λ-doublet levels and renormalized before being fit to a statistical prior distribution for which the excess energy, E_{exc}, was the variable parameter and the term values for the O_2 partner are calculated from previously reported molecular constants. The outcome of such a fit following overtone excitation is presented in Figure 3 of Murray et al.[13] Following excitation of the fundamental OH stretch of *trans*-HOOO, the OH $X^2\Pi$, $v = 0$ distribution is reasonably well described by a statistical prior distribution and the fit returns a value of $E_{exc} = 1060 \pm 40$ cm^{-1} (2σ uncertainty). In the case of a statistical unimolecular dissociation, knowledge of the excess energy and the total energy available to the system allows the dissociation energy, D_0, for the system to be calculated. The total energy available to the system is the sum of the photon energy used for excitation, $h\nu_{IR} = 3571.8$ cm^{-1}, and the internal energy of *trans*-HOOO, E_{int}(HOOO), which is calculated to be 3.8 cm^{-1} based on the energy of the ground-state level from which the IR transition originates. Thus, D_0 is calculated to be 2520 ± 40 cm^{-1} or 7.20 ± 0.11 kcal mol^{-1}.

A similar analysis can be performed for the products of *trans*-HOOO dissociation following excitation of the OH stretch overtone. As discussed previously, the OH $X^2\Pi$ products are formed exclusively in $v = 1$ and a normal prior distribution necessarily gives greater weight to $v = 0$ as a consequence of the translational degrees of freedom which scale as the square root of the excess energy. Since OH $X^2\Pi$, $v = 0$ is not observed in the experiment, the calculation was constrained to preserve one quantum of vibration in the OH fragment, by simply excluding these rotational levels and correspondingly reducing the energy of the OH $X^2\Pi$, $v \geq 1$ term values. Unsurprisingly, given the obvious similarities of the rotational distributions shown in Figure 4, this analysis gives a very similar excess energy, $E_{exc} = 1049 \pm 56$ cm^{-1}, but results in a smaller dissociation energy $D_0 = 2363 \pm 56$ cm^{-1} or 6.76 ± 0.16 kcal mol^{-1}. This reduction of the available energy is a straightforward consequence of the anharmonicity of the OH stretch in *trans*-HOOO. As we have discussed previously,[13] an upper limit to the dissociation energy is better determined by the energetically highest open OH $X^2\Pi$ product and applying simple conservation of energy, assuming negligible partitioning of the available energy into relative translation and the internal degrees of freedom of the O_2 partner fragment. Following excitation of the fundamental OH stretch, the $X^2\Pi_{1/2}$, $v = 0$, $N = 8$, f level at 1367.6 cm^{-1} is the highest observed, providing an upper limit to D_0 of 2208 cm^{-1}. A tighter constraint on the dissociation energy is obtained using the energetically highest level observed following excitation of the overtone OH stretch, $X^2\Pi_{3/2}$, $v = 1$, $N = 8$, e at 4840.2 cm^{-1}; as reported previously,[13] $D_0 \leq 2140$ cm^{-1} or 6.12 kcal mol^{-1}.

The analysis above relies on the assumption that the partitioning of energy into internal motion of the O_2 partner and translational recoil is relatively unimportant. In fact, the IR photon used to excite $2\nu_{OH}$ provides sufficient energy to produce the highest observed OH $X^2\Pi$ product state in coincidence with

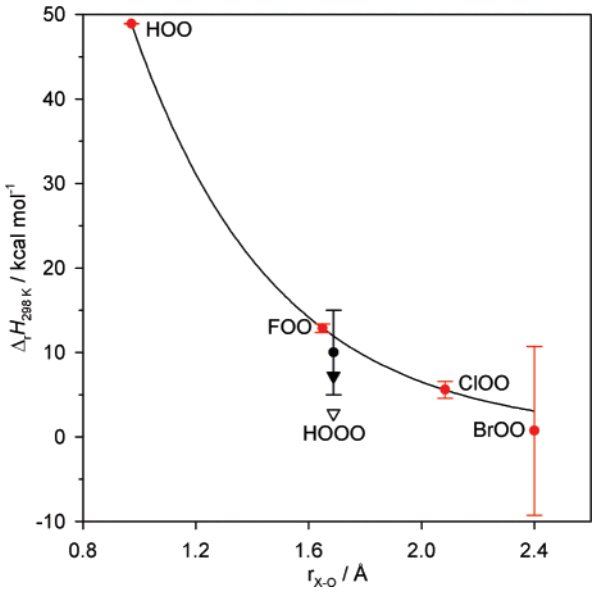

Figure 5. Plot of the enthalpies of dissociation ($\Delta_r H_{298K}$) versus X−O bond lengths for a homologous series of XOO molecules, where X is H, F, Cl, or Br as indicated. Recommended $\Delta_r H_{298K}$ values (with 1σ uncertainties) are taken from the NASA/JPL compilation[32] and indicated by red circles. The experimental measurement of $\Delta_r H_{298K}$ for HOOO by Speranza is indicated by a black circle.[19] The closed and open triangles represent upper limits to the dissociation enthalpies derived from IR action spectroscopy,[13] with the assumption that the O_2 partner fragment is formed coincidentally in $v = 0$ or $v = 1$, respectively. Geometric parameters are taken from several sources for HOO,[39] FOO,[40] ClOO,[37] BrOO,[41] and HOOO.[18]

O_2 $X^3\Sigma_g^-$, $v = 1$, with a corresponding decrease in the upper limit binding energy to $D_0 \leq 584$ cm^{-1} or 1.67 kcal mol^{-1}. We consider this to be an unreasonably small value for D_0, primarily given the central O−O bond length in HOOO. The asymmetric halogen oxides are isoelectronic with HOOO and in conjunction with the hydroperoxy radical form a homologous series, XOO, where X is H, F, Cl, or Br, which allows examination of the relationship between X−O bond length and the enthalpy of dissociation. Figure 5 illustrates this relationship, plotting $\Delta_r H_{298K}$ for XOO → X + O_2 dissociation[32] as a function of the bond length, r_{X-O}. Given that the central O−O bond in *trans*-HOOO is 1.688 Å,[18] we would anticipate a $\Delta_r H_{298K}$ of 11.9 kcal mol^{-1}, which is equivalent to D_0 of 10.8 kcal mol^{-1} after correction for thermal contributions. While this $\Delta_r H_{298K}$ is in good agreement with the value of 10 ± 5 kcal mol^{-1} inferred by Speranza,[19,33] it is inconsistent with our experimental observations as excitation of the fundamental OH stretch vibration (3568 cm^{-1} or 10.2 kcal mol^{-1}) would provide insufficient energy to cause dissociation. Production of O_2 $X^3\Sigma_g^-$, $v = 0$ cofragments leads to $\Delta_r H_{298K} \leq 7.3$ kcal mol^{-1} for HOOO after inclusion of thermal corrections, which lies slightly below the curve but is in reasonably good agreement. The smaller upper limit to D_0 implied by coincidental production of O_2 $X^3\Sigma_g^-$, $v = 1$ leads to $\Delta_r H_{298K} \leq 2.8$ kcal mol^{-1}, which appears too far from the trend to be reasonable. Furthermore, the rotational distributions show no evidence of bimodality, which may be expected if O_2 were produced in both $v = 0$ and $v = 1$, while exclusive production of the latter is considered unlikely in the absence of any near resonance and the requirement for a change of two vibrational quanta. Perhaps the most compelling evidence against the lower value of D_0 is purely empirical; production of HOOO in the expansion is copious.

While the overall rotational distributions in both spin−orbit manifolds can be modeled statistically, one of the most striking

features of the product state distributions displayed in Figure 4 is distinctly nonstatistical: namely, a strong propensity for the formation of Π(A′) Λ-doublets. This is manifest in the greater intensity of main branch P- and R-type transitions, which probe population in F_{1e} and F_{2f} levels, relative to main branch Q-type transitions, which probe F_{1f} and F_{2e} levels. In this notation, the labels e and f refer to the rotationless parity of the level, while from a dynamical perspective it is more useful to consider the symmetry of these levels with respect to the plane defined by the rotation of the nuclei. In the high *J* limit (or, for convenience, the high *N* limit) when this plane is well-defined and the molecule can be described using Hund's case (b) coupling, the F_{1e} and F_{2f} Λ-doublets can be labeled as Π(A′) while F_{1f} and F_{2e} are Π(A″).[34] However, for the low to moderate rotational levels populated in the present experiment, OH $X^2\Pi$ is best described in terms of intermediate Hund's case (a) and (b) coupling, and thus any given Λ-doublet is an admixture of the Π(A′) and Π(A″) limiting cases. A fundamental question arising from this interpretation, as discussed by Andresen and Rothe,[35] is concerned with the extent to which the *N*-dependence of the observed population ratio (or degree of alignment) is a dynamical effect as opposed to being simply a consequence of incomplete orbital alignment at small nuclear rotation. The electronic effect of wave function mixing at low *N*, referred to as the degree of electron alignment and denoted by $(DEA)_{el}$, is an intrinsic property of OH and affects the measurability of a Λ-doublet propensity at smaller values of the nuclear rotation quantum number. The value of $(DEA)_{el}$ is readily calculated given knowledge of the spin−orbit coupling and rotational constants for OH $X^2\Pi$ and is directly related to the molecule undergoing transition from Hund's case (a) to case (b) coupling with increasing rotation of the nuclear framework.[35] The experimentally observed Λ-doublet propensity is also identified as the degree of electron alignment, or $(DEA)_{exp}$, and is defined[35] as

$$(\mathrm{DEA})_{\mathrm{exp}} = \frac{P_{\Pi(\mathrm{A}')} - P_{\Pi(\mathrm{A}'')}}{P_{\Pi(\mathrm{A}')} + P_{\Pi(\mathrm{A}'')}}$$

where *P* represents the population in the Λ-doublet specified by the subscript. In the limit of complete orbital alignment, $(DEA)_{exp}$ can take the limiting values of +1 or −1. Dividing $(DEA)_{exp}$ by $(DEA)_{el}$ effectively removes any *N* dependence of the apparent alignment caused by the intrinsically incomplete orbital alignment at low *N*; this quotient is called the reduced DEA, or $(DEA)_{red}$.

In Figure 6, we show $(DEA)_{red}$ plotted as a function of *N* for OH products in the F_1 spin−orbit manifold following excitation of *trans*-HOOO in the fundamental and overtone OH stretch regions. The corresponding data for the F_2 spin−orbit manifold are omitted for clarity but qualitatively show the same behavior. Figure 6 makes explicit the unambiguous propensity for the production of Π(A′) levels. Indeed, the experimental data indicate not only that there is a preference for in-plane alignment of the unpaired electron, but also that it is effectively *maximally aligned*. The degree of alignment observed is unaffected by the number of quanta of OH stretch initially excited in *trans*-HOOO, while the use of $(DEA)_{red}$ demonstrates that the alignment is independent of the rotational quantum number of the product OH $X^2\Pi$. The weighted mean $(DEA)_{red}$ over all observed *N* levels following excitation of the fundamental OH stretch is 0.91 ± 0.03, while that of the overtone is 0.95 ± 0.08 (2σ uncertainties). The separability of the rotational motion, which is of course the consequence of the torque applied to the OH fragment during predissociation, and the orientation of the orbital lobe containing the unpaired electron suggest that the observed propensity is stereochemical rather than dynamical. The propensity for OH $X^2\Pi$ products to be formed in levels of Π(A′) symmetry can be rationalized as arising from a planar dissociation in which the symmetry of the orbital containing the electron whose fate is to be unpaired in the OH moiety is maintained during the dissociation, viz. the chemical bonding in HOOO is due to electrons in an orbital of a′ symmetry.

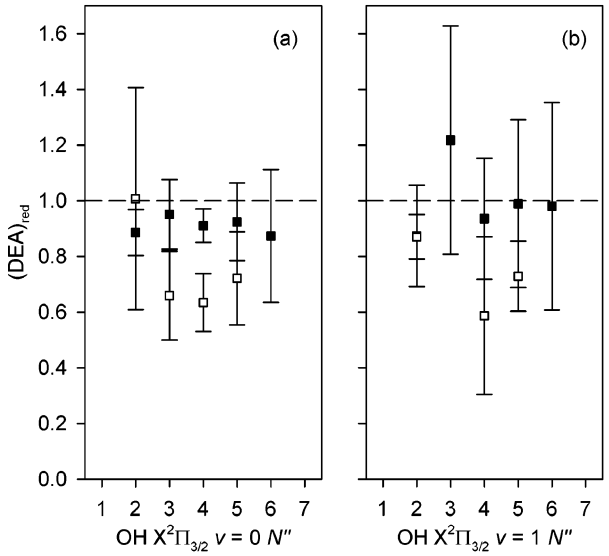

Figure 6. Reduced degree of electron alignment, $(DEA)_{red}$, observed in OH $X^2\Pi_{3/2}$ vibrational predissociation products following excitation in the OH stretch fundamental (a) and overtone (b) regions of HOOO. Products of excitation on the R(3) feature of the *trans*-HOOO conformer (■) and the unstructured *cis*-HOOO conformer (□) as indicated on the spectra in Figure 2 are shown. That $(DEA)_{red}$ is close to its limiting value of +1 indicates a propensity for production of Π(A′) Λ-doublets for which the unpaired electron lies in the plane of nuclear rotation.

A qualitative molecular orbital diagram illustrating the bonding in HOOO is displayed in Figure 7. The interaction of OH $X^2\Pi$ and O_2 $X^3\Sigma_g^-$ in C_s geometries gives rise to four electronic surfaces of ^{2}A′, ^{2}A″, ^{4}A′, and ^{4}A″ symmetry, of which the ^{2}A″ state is the electronic ground state of HOOO. Although we focus on the interaction of OH and O_2 in their electronic ground states, it is worth noting in passing that the low-lying (7918 cm^{-1}) O_2 $a^1\Delta_g$ state gives rise to a further four surfaces, two of ^{2}A′ and two of ^{2}A″ symmetry, and inclusion of spin−orbit coupling will increase the number of surfaces still further. In HOOO X^2A″, a weak covalent bond is formed by the interaction of the unpaired electrons in the in-plane O_2 $1\pi_g$ (7a′) and OH 1π (4a′) orbitals; it is the resultant HOOO 10a′ bonding orbital, as illustrated in Figure 7, that maintains its symmetry upon dissociation and thus the propensity for vibrational predissociation on the ground-state surface to produce OH $X^2\Pi$ in Π(A′) Λ-doublets. The remaining unpaired electron gives the HOOO electronic ground state its ^{2}A″ character, residing as it does in the 3a″ out-of-plane molecular orbital. This orbital has much of the character of the $1\pi_g$ (2a″) O_2 antibonding orbital, although the interaction with the OH 1π (1a″) lone pair causes it to be localized on the terminal O atom. Exchange repulsion between the OH 1π (1a″) lone pair and the $1\pi_u$ (1a″) bonding orbitals on O_2 (which are not shown in Figure 7) becomes increasingly important at shorter internuclear separations and thus ensures that the O−O bond length is extended, in analogy to the asymmetric halogen dioxides.[36] The relative weakness of the central O−O bond in the XOO systems is

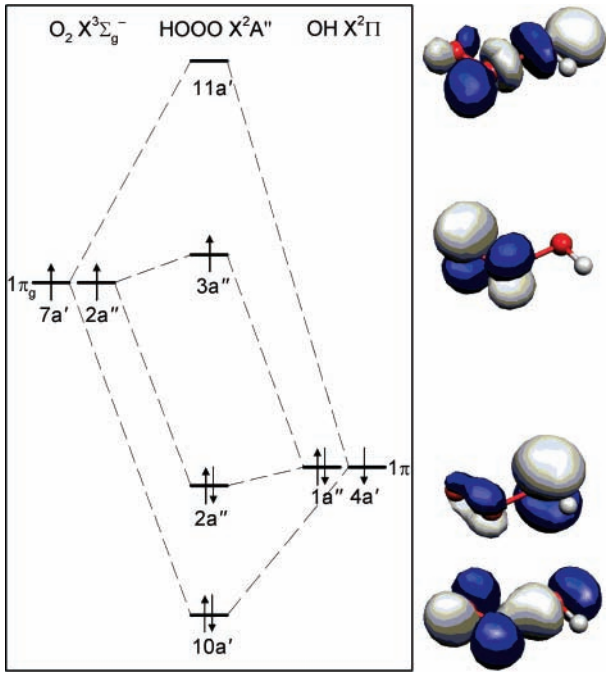

Figure 7. Schematic molecular orbital diagram describing the anticipated bonding in HOOO $\tilde{X}^2A''$. The interaction between the half-filled, in-plane lobes of the O_2 $1\pi_g$ and OH 1π orbitals gives rise to the primary bonding orbital, labeled 10a′, which is analogous to a pσ bond in a diatomic molecule. The unpaired electron resides in the 3a″ orbital, which retains much of the character of the O_2 $1\pi_g$ orbital it descends from, but is more localized on the terminal O atom. Hartree−Fock orbitals calculated at the experimental geometry are shown on the right to provide a qualitative representation of the expected frontier orbitals in HOOO.

furthermore a direct consequence of configuration interaction in the electronic structure, as the second largest contribution to the total wave function arises from an electronic configuration of distinctly antibonding character.[25,37]

C. Identification of the Unstructured Bands as *cis*-HOOO. An unambiguous identification of the unstructured features observed in both the fundamental and overtone regions of the IR action spectra is more problematic than that of the structured feature. Previously,[13] we suggested that the feature in the overtone region could be due to absorption by the *cis*-HOOO conformer, and we present this argument more fully here, with additional reference to the action spectrum in the fundamental OH stretch region and the detailed fine-structure resolved product state distributions.

One initial proposition, before observation of the fundamental band and based upon consideration of the large number of low-lying electronic states that correlate to OH $X^2\Pi$ and O_2 $X^3\Sigma_g^-$ or O_2 $a^1\Delta_g$ products, was an electronic excitation to a state that was either repulsive or predissociative. This can now be categorically ruled out as the unstructured feature is clearly present in both the fundamental and overtone OH stretch regions with similar intensity, and additionally in the OD stretch overtone of DOOO.[13] Indeed, the presence of a similar feature in the OH stretch fundamental region allows us confidently to assign these features to OH stretching vibrations. The centers of the line shape functions used to represent the unstructured features suggest band origins of 3565.4 and 6968.3 cm^{-1} and thus small red shifts from the *trans*-HOOO band origins. The overall widths of these features are also comparable to the widths of the *trans*-HOOO bands, which suggests that the absorbing species has similar rotational constants, consistent with *cis*-HOOO. A simulation using the calculated rotational constants

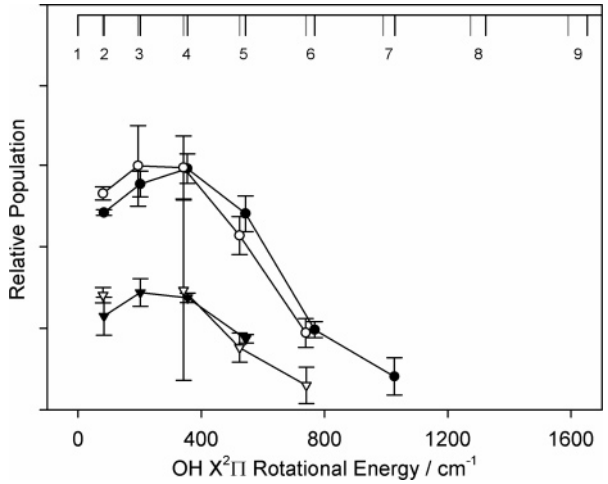

Figure 8. Nascent OH $X^2\Pi_{3/2}$ fine-structure resolved product state distributions as a function of rotational energy after excitation of the unstructured absorption features, tentatively assigned to *cis*-HOOO. Excitation in the fundamental OH stretch region at 3563.1 cm^{-1} leads to $v = 0$ products indicated by filled symbols and in the overtone region at 6965.4 cm^{-1} leads to $v = 1$ products indicated by open symbols. Circles represent the populations in F_{1e} and F_{2f} Λ-doublet levels, which are also indicated Π(A′), and triangles represent the F_{1f} and F_{2e} level populations, also indicated Π(A″). $(DEA)_{red}$ values calculated from these data are shown in Figure 6. The distributions are normalized to unity over all common observed fine-structure levels, and the error bars represent (2σ) uncertainties from repeated measurements.

for *cis*-HOOO, red-shifted and homogeneously broadened to have a line width of 5 cm^{-1}, provides an equally satisfactory representation of the unstructured band and would correspond to an excited-state lifetime of ∼1 ps (vide infra).

Consideration of the nascent OH $X^2\Pi$ product state distributions following excitation of the unstructured features provides further evidence for *cis*-HOOO. These were recorded in an analogous manner to that described previously for *trans*-HOOO, by scanning the UV probe laser wavelength over various transitions of the OH $A^2\Sigma^+ - X^2\Pi$ band with the IR pump laser operating at a fixed frequency. Given the absence of any propensity for production of either spin−orbit manifold of OH $X^2\Pi$ after excitation of the structured feature, only levels within the F_1 spin−orbit manifold were probed. The IR laser was tuned to be resonant near the peak of the unstructured absorption features, the criterion for choosing the absolute wavelength being optimization of signal while discriminating between the unstructured absorption and any underlying structured absorption by *trans*-HOOO. Consequently, the IR laser was fixed at 3563.1 and 6965.4 cm^{-1} in the vicinities of the fundamental and overtone OH stretch transitions, respectively. The rotational state distributions obtained following excitation of the unstructured features are displayed in Figure 8, and these data are directly comparable to those in Figure 4a, which were obtained following excitation of the structured band.

Excitation of the unstructured band adjacent to the overtone leads exclusively to formation of OH $X^2\Pi$, $v = 1$ products as was observed following overtone excitation of *trans*-HOOO. Thus, vibrational predissociation of the absorbing species occurs sufficiently fast that only a single quantum of OH stretch excitation is lost. Again in analogy to dissociation of *trans*-HOOO, the rotational distributions within each vibrational manifold are identical within the uncertainty of the measurements, peaking around $N = 3-4$, irrespective whether the fundamental or overtone OH stretch is initially excited. Furthermore, the rotational distributions shown in Figure 8 are qualitatively similar to those displayed in Figure 4a and an

N-independent propensity for production of $\Pi(A')$ Λ-doublets is also observed, albeit less strongly; weighted mean $(DEA)_{red}$ values are 0.67 ± 0.05 and 0.82 ± 0.05 after fundamental and overtone OH stretch excitation, respectively. Overall, and taken in conjunction with the spectroscopic observations, this is strongly suggestive that the IR absorbing species is also HOOO, and the decreased values for the mean values of $(DEA)_{red}$ suggest a degree of nonplanarity during dissociation.

Experiments were performed in which attempts were made to alter the temperature of the free-jet expansion to examine the possibility that hot bands of *trans*-HOOO could be responsible for the unstructured bands. This was achieved by replacing the Ar carrier gas with He, varying the pulsed valve stagnation pressure, or by moving the detection region to smaller values of *x*/*D*, wherein the collisional cooling of the expansion is less complete. However, within the limits of our experimental uncertainty, while the absolute signal intensity was variable, the relative intensities of the unstructured and structured features were unchanged despite these changes in the experimental conditions. Given this constancy under different temperature conditions, *trans*-HOOO hot bands are an unsatisfactory explanation for the origin of these features.

We assign the unstructured features to *cis*-HOOO, which is expected to have a similar dissociation energy and hence to be present in similar quantities to *trans*-HOOO in the supersonic free-jet expansion. Indeed, the unstructured bands account for around one-third of the total intensity in both the fundamental and overtone regions of the spectrum. However, density functional theory calculations[21,24] of the vibrational frequencies predict the OH stretch frequency of *cis*-HOOO to be red-shifted with respect to *trans*-HOOO, which presumably is caused by intramolecular hydrogen bonding. Following Fabian et al.,[24] an anharmonic frequency analysis at the B3LYP/cc-pVTZ level of theory predicts a 27 cm^{-1} red shift for the OH stretch fundamental of *cis*-HOOO with respect to *trans*-HOOO and a shift of 53 cm^{-1} in the overtone. Consequently, the IR laser was scanned up to 200 cm^{-1} to lower frequency with respect to the fundamental and overtone band origins, but no features were observed in the action spectra that could be attributed to *cis*-HOOO. At this level of theory, the central O−O bond lengths in *cis*-HOOO and *trans*-HOOO were calculated to be 1.502 and 1.544 Å, respectively, in both cases significantly shorter than the experimental determination for *trans*-HOOO of 1.688 Å by Suma et al.[18] The degree of hydrogen bonding and its influence on the vibrational frequency of the OH stretch mode is thus exaggerated in the calculations, primarily as a consequence of the method failing to provide an accurate geometry.

The absence of rotational structure in the *cis*-HOOO bands is more difficult to explain. As suggested previously, homogeneous lifetime broadening would indicate a lifetime of ~1 ps for the vibrationally excited state. The smaller value of $(DEA)_{red}$ observed following excitation of the unstructured features is consistent with some loss of planarity during the dissociation, which may indicate that the OH stretch vibration is strongly coupled to torsional motion. There is some evidence for this in the B3LYP/cc-PVTZ calculations alluded to earlier such that the anharmonic coupling constant between OH stretch and HOOO torsion is only 5 cm^{-1} for *trans*-HOOO and 39 cm^{-1} for *cis*-HOOO, likely due to the presence of the intramolecular hydrogen bond. Therefore, it is possible that torsional excitation enhances the IVR and/or predissociation rate, giving rise to lifetime broadening and thus absence of rotational structure in the *cis*-HOOO spectrum. An analogous situation was observed for HOONO, for which the spectrum attributed to the hydrogen-bonded cis−cis conformer was unstructured, while the trans−perp conformer exhibited rotational structure.[38] Clearly, it would be highly desirable to have high-level multireference calculations characterizing the torsional potential energy surface in the ground and vibrationally excited states.

Conclusions

The HOOO radical has been produced by three-body association of OH $X^2\Pi$ and O_2 $X^3\Sigma_g^-$ in the collisional region of a supersonic expansion and characterized using IR action spectroscopy in the OH stretch fundamental and overtone regions. In both spectral regions, an absorption feature comprising a rotationally structured feature and an unstructured feature lying very close to free OH were observed. The former can be assigned confidently to the *trans*-HOOO conformer using rotational constants previously determined from microwave studies, while the unstructured features are assigned to the *cis*-HOOO conformer. OH $X^2\Pi$ product state distributions (vibrational, rotational, and fine-structure) reveal that vibrational predissociation occurs exclusively with loss of a single quantum of OH stretch excitation and with a strong propensity for the production of $\Pi(A')$ Λ-doublets, particularly from *trans*-HOOO. This is interpreted as indicating planar dissociation in which the symmetry of the bonding orbital is retained.

Acknowledgment. This work was supported by the Chemistry Division of the National Science Foundation. C.M. acknowledges financial support from the Dreyfus Postdoctoral Program in Environmental Chemistry.

References and Notes

(1) Wentworth, P., Jr.; Wentworth, A. D.; Zhu, X.; Wilson, I. A.; Janda, K. D.; Eschenmoser, A.; Lerner, R. A. *Proc. Natl. Acad. Sci. U.S.A.* **2003**, *100*, 1490.

(2) Plesničar, B.; Cerkovnik, J.; Tekavec, T.; Koller, J. *J. Am. Chem. Soc.* **1998**, *120*, 8005.

(3) Plesničar, B.; Cerkovnik, J.; Tekavec, T.; Koller, J. *Chem.−Eur. J.* **2000**, *6*, 809.

(4) Plesničar, B.; Tuttle, T.; Cerkovnik, J.; Koller, J.; Cremer, D. *J. Am. Chem. Soc.* **2003**, *125*, 11553.

(5) Charters, P. E.; Macdonald, R. G.; Polanyi, J. C. *Appl. Opt.* **1970**, *10*, 1747.

(6) Klenerman, D.; Smith, I. W. M. *J. Chem. Soc., Faraday Trans.* **1987**, *83*, 229.

(7) Wayne, R. P. *Chemistry of Atmospheres*, 3rd ed.; Oxford University Press: New York, 2000.

(8) Dodd, J. A.; Lipson, S. J.; Blumberg, W. A. M. *J. Chem. Phys.* **1990**, *92*, 3387.

(9) Dodd, J. A.; Lipson, S. J.; Blumberg, W. A. M. *J. Chem. Phys.* **1991**, *95*, 5752.

(10) D'Ottone, L.; Bauer, D.; Campuzano-Jost, P.; Fardy, M.; Hynes, A. J. *Phys. Chem. Chem. Phys.* **2004**, *6*, 4276.

(11) McCabe, D. C.; Smith, I. W. M.; Rajakumar, B.; Ravishankara, A. R. *Chem. Phys. Lett.* **2006**, *421*, 111.

(12) Sridharan, U. C.; Klein, F. S.; Kaufman, F. *J. Chem. Phys.* **1985**, *82*, 592.

(13) Murray, C.; Derro, E. L.; Sechler, T. D.; Lester, M. I. *J. Phys. Chem. A* **2007**, *111*, 4727.

(14) Cacace, F.; De Petris, G.; Pepi, F.; Troiani, A. *Science* **1999**, *285*, 81.

(15) Nelander, B.; Engdahl, A.; Svensson, T. *Chem. Phys. Lett.* **2000**, *332*, 403.

(16) Cooper, P. D.; Moore, M. H.; Hudson, R. L. *J. Phys. Chem. A* **2006**, *110*, 7985.

(17) Zheng, W.; Jewitt, D.; Kaiser, R. I. *Phys. Chem. Chem. Phys.* **2007**, *9*, 2556.

(18) Suma, K.; Sumiyoshi, Y.; Endo, Y. *Science* **2005**, *308*, 1885.

(19) Speranza, M. *Inorg. Chem.* **1996**, *35*, 6140.

(20) Denis, P. A.; Kieninger, M.; Ventura, O. N.; Cachau, R. E.; Diercksen, G. H. F. *Chem. Phys. Lett.* **2003**, *377*, 483.

(21) Jungkamp, T. P. W.; Seinfeld, J. H. *Chem. Phys. Lett.* **1996**, *257*, 15.

(22) Yu, H. G.; Varandas, A. J. C. *Chem. Phys. Lett.* **2001**, *334*, 173.
(23) Setokuchi, O.; Sato, M.; Matuzawa, S. *J. Phys. Chem. A* **2000**, *104*, 3204.
(24) Fabian, W. M. F.; Kalcher, J.; Janoschek, R. *Theor. Chem. Acc.* **2005**, *114*, 182.
(25) Feller, D.; Dixon, D. A. *J. Phys. Chem. A* **2003**, *107*, 9641.
(26) Colin, R.; Coheur, P.-F.; Kiseleva, M.; Vandaele, A. C.; Bernath, P. F. *J. Mol. Spectrosc.* **2002**, *214*, 225.
(27) Pickett, H. M. *J. Mol. Spectrosc.* **1991**, *148*, 371.
(28) Takahashi, K.; Sugawara, M.; Yabushita, S. *J. Phys. Chem. A* **2005**, *109*, 4242.
(29) Konen, I. M.; Li, E. X. J.; Stephenson, T. A.; Lester, M. I. *J. Chem. Phys.* **2005**, *123*, 204318.
(30) Cleary, P. A.; Dempsey, L. P.; Murray, C.; Lester, M. I.; Kłos, J.; Alexander, M. H. *J. Chem. Phys.* **2007**, *126*, 204316.
(31) Guyer, D. R.; Huwel, L.; Leone, S. R. *J. Chem. Phys.* **1983**, *79*, 1259.
(32) Sander, S. P.; Friedl, R. R.; Golden, D. M.; Kurylo, M. J.; Moortgat, G. K.; Wine, P. H.; Ravishankara, A. R.; Kolb, C. E.; Molina, M. J.; Finlayson-Pitts, B. J.; Huie, R. E.; Orkin, V. L. *Chemical kinetics and photochemical data for use in atmospheric studies: Evaluation number 15;* NASA JPL Publication 06-02; Jet Propulsion Laboratory, California Institute of Technology: Pasadena, CA, 2006.
(33) Speranza, M. *J. Phys. Chem. A* **1998**, *102*, 7535.
(34) Alexander, M. H.; Andresen, P.; Bacis, R.; Bersohn, R.; Comes, F. J.; Dagdigian, P. J.; Dixon, R. N.; Field, R. W.; Flynn, G. W.; Gericke, K.-H.; Grant, E. R.; Howard, B. J.; Huber, J. R.; King, D. S.; Kinsey, J. L.; Kleinermanns, K.; Kuchitsu, K.; Luntz, A. C.; McCaffery, A. J.; Pouilly, B.; Reisler, H.; Rosenwaks, S.; Rothe, E. W.; Shapiro, M.; Simons, J. P.; Vasudev, R.; Wiesenfeld, J. R.; Wittig, C.; Zare, R. N. *J. Chem. Phys.* **1988**, *89*, 1749.
(35) Andresen, P.; Rothe, E. W. *J. Chem. Phys.* **1985**, *82*, 3634.
(36) Filatov, M.; Cremer, D. *Phys. Chem. Chem. Phys.* **2003**, *5*, 2320.
(37) Suma, K.; Sumiyoshi, Y.; Endo, Y. *J. Chem. Phys.* **2004**, *121*, 8351.
(38) Fry, J. L.; Nizkorodov, S. A.; Okumura, M.; Roehl, C. M.; Francisco, J. S.; Wennberg, P. O. *J. Chem. Phys.* **2004**, *121*, 1432.
(39) Lubic, K. G.; Amano, T.; Uehara, H.; Kawaguchi, K.; Hirota, E. *J. Chem. Phys.* **1984**, *81*, 4826.
(40) Yamada, C.; Hirota, E. *J. Chem. Phys.* **1984**, *80*, 4694.
(41) Suma, K.; Sumiyoshi, Y.; Endo, Y. *J. Chem. Phys.* **2005**, *123*, 024312.